Interfacial Polymerization Kinetics of Polyurea Microcapsules Formed Using Hexamethylene Diisocyanate Biuret Low Viscosity Isocyanate

Pablo Canamas, Nathan Gozzi, Jiupeng Du, Pierrette Guichardon

Pablo Canamas
Nathan Gozzi
Jiupeng Du
Pierrette Guichardon*

Interfacial Polymerization Kinetics of Polyurea Microcapsules Formed Using Hexamethylene Diisocyanate Biuret Low Viscosity Isocyanate

For cosmetic industrial applications, polyurea microcapsules were formed by using hexamethylene diisocyanate biuret low viscosity (HDB-LV) and three different amines: ethylenediamine (EDA), guanidine (GUA), and hexamethylenediamine (HMDA). Toluene droplets containing dissolved HDB-LV were formed by an oil-in-water emulsion before being poured into a water phase containing the required excess of amine. The pH of the aqueous phase was fitted through time to calculate the kinetic constant k' and the diffusion constant D_B through the polyurea shell when possible. At 60 °C, EDA and HMDA follow a pure kinetic regime, whereas GUA follows a combination of kinetic and diffusion regimes. The presented kinetic data shows that HDB-LV is a promising nontoxic isocyanate for cosmetic encapsulation.

Keywords: Diffusion, Interfacial polymerization, Kinetics, Modeling, Polyurea microcapsules

Received: November 02, 2022; *revised:* December 16, 2022; *accepted:* January 09, 2023

DOI: 10.1002/ceat.202200543

1 Introduction

Interfacial polymerization (IP) is a technique for encapsulation of active compounds with a large scope of applications [1, 2], notably for containment or controlled release in the cosmetic [3] and soil management industries [4, 5], but also for thin-film composite membranes [6]. Polyurea microcapsules are amongst the most studied today because of their high molecular weight [7] and controlable size for a wide range of release properties [8–10].

The easy synthesis of polyurea microcapsules by IP results from the reaction between a diisocyanate and a diamine (Fig. 1). Each monomer is dissolved in one of two immiscible solvents: water for the amine and an organic solvent for the isocyanate. The reaction takes place at the interface, where the polyurea accumulates as a film because it is insoluble in both phases. As the two phases initially form an emulsion, polyurea films form shells around the encapsulated oil phase.

Previous reports [11–15] classically use hexamethylene diisocyanate (HDI) as the isocyanate monomer. However, HDI is toxic [16] and not ideal for our targeted cosmetic applications. Therefore, we focus on the nontoxic derivative hexamethylene diisocyanate biuret low viscosity (HDB-LV, Fig. 1). The nontoxicity is due to the size of HDB-LV, which has longer carbon chains than HDI monomer, so it cannot penetrate through human skin and is also nonvolatile [8]. This prepolymer is suitable for emulsification, but the kinetic behavior of the system HDB-LV/amine remains undocumented.

After a few experiments, it appeared that reactions of HDB-LV with amines are extremely slow at room temperature. To reach decent reaction times of around an hour, the temperature was increased to 60 °C. A stoichiometric excess of amine was used to avoid the parasite hydrolysis of isocyanate (Fig. 1), which is not negligible at 60 °C [17].

With the above background, Sect. 2 describes how different polyurea microcapsules were synthesized from nontoxic HDB-LV isocyanate, by using a two-step IP protocol composed of emulsification followed by polymerization. Three different amines were tested: ethylenediamine (EDA), guanidine (GUA), and hexamethylenediamine (HMDA). After tracking the pH of the aqueous phase with a probe, in Sect. 3 the work of Yadav et al. [13], which also inspired refs. [7, 11, 14], was extended to propose an adapted modeling framework for the reaction kinetics. The model fits the normalized H^+ concentration $[H^+]$, retrieving a kinetic constant k'[1)] and a diffusion constant D_B, depending on the regime that drives the reaction (kinetic or a combination of kinetic and diffusion regimes). Considering the experimental results, Sect. 4 discusses which parameters play a crucial role in the kinetics for each amine and explains why the

1) List of symbols at the end of the paper.

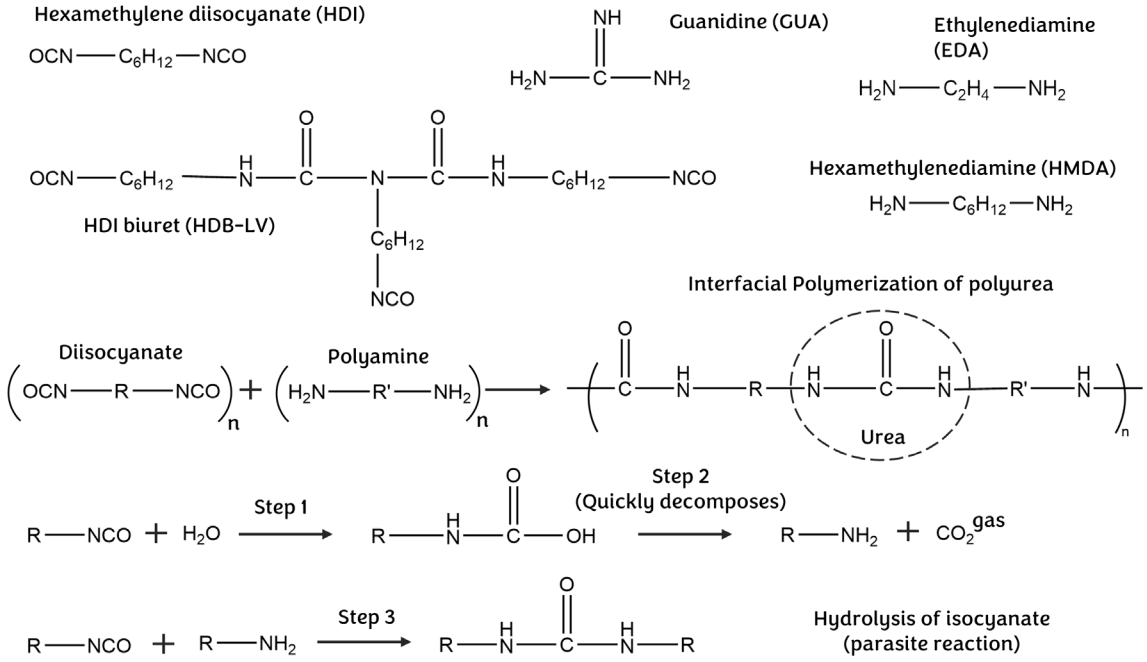

Figure 1. Chemical formula of the different chemicals of the system and main reactions.

reaction times are long for GUA. Numerical precautions that need to be taken when working with an excess of amine are emphasized. Finally, Sect. 5 presents the best options to optimise the studied IP reaction made with HDB-LV for cosmetic applications.

2 Materials and Methods

2.1 Chemicals

The isocyanate monomer HDB-LV (23.5 ± 1.0 wt % of isocyanate groups and < 0.3 wt % of HDI, Vencorex) was dissolved in Toluene (99.85 %, Fisher). Hexamethylenediamine (98 %, Sigma Aldrich), guanidine carbonate (99+ %, Sigma Aldrich), and ethylenediamine (99+ %, Sigma Aldrich) were dissolved in distilled water. The emulsions were stabilized with sodium dodecyl sulfate (99+ %, Sigma Aldrich).

2.2 Adapting Existing Protocols to Work with an Excess of Amine

If the ratio of the molar amount of isocyanate (NCO) reactive groups to the molar amount of amino (NH_2) reactive groups R is > 1, after complete consumption of amine by the IP reaction the remaining isocyanate groups are hydrolyzed by water and CO_2 is released (Fig. 1). This causes a parasitic drop of the pH to acidic values, and thus it is impossible to track the amine concentration with the pH. This parasite reaction is negligible at 25 °C for fast IP reactions [13] but not at 60 °C [17].

Therefore, $R < 1$ was set to avoid this inconvenience. Thus, only the desired IP occurs until all the isocyanate is converted to polyurea, and the residual amine does not participate in other reactions. The temperature was fixed at 60 °C as a reference, because it is a good compromise for cosmetic applications. It is fast enough and does not deteriorate the cosmetic organic compounds targeted for encapsulation. Increasing the temperature also favors the faster kinetic reaction, which is isocyanate + amine, as isocyanate has a higher selectivity towards basic compounds than water.

2.3 Experimental Protocol

Microcapsules were prepared by IP. The first step is emulsification of the toluene phase containing the HDB-LV monomer mixed with a water phase and sodium dodecyl sulfate (SDS) surfactant. Immediately thereafter, a controlled volume of this emulsion was poured into a stirred phase of water + amine to start the IP reaction at the initial time t_0 (Fig. 2). Toluene is only used here as an ideal inert solvent for the kinetic study. For industrial applications it can be switched to cosmetic

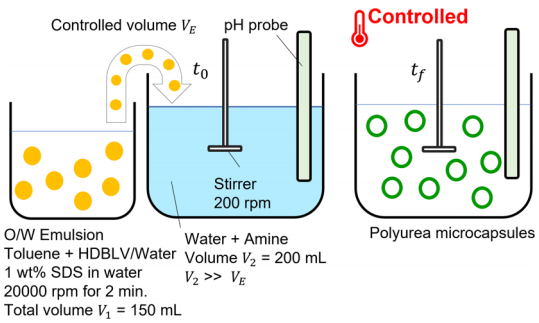

Figure 2. Experimental protocol for the formation of polyurea microcapsules.

solvents such as esters to form similar capsules. However, esters lead to parasite reactions with a small portion of the amines, forming amides and alcohols, which cause a pH drop and hinder kinetic measurements.

Different initial concentrations of amines in the aqueous phase (0.0125–0.1 wt %) and of isocyanate in the organic phase (20–50 wt %) were tested. They correspond to an R range of 0.33–0.87. For the specific case of EDA, different temperatures of 40, 60 (reference), and 80 °C were also tested.

For all experiments, 50 mL of toluene with an initial molar HDB-LV concentration C_{A0} was mixed with an aqueous phase of 100 mL of water containing 1 wt % of SDS surfactant. An emulsion of volume V_1 = 150 mL was made using an Ultraturrax device (T25 easy clean control, IKA) at 20 000 rpm for 2 min in a 250-mL beaker.

Immediately thereafter, a controlled volume V_E of the resulting emulsion was poured into another 250-mL beaker containing V_2 = 200 mL of water with a controlled concentration C_{T0} of amine at a monitored temperature and stirred at 200 rpm. Volume V_E was always much smaller than V_2 so that the dilution effect on the pH could be neglected.

The different values of C_{A0} and V_E chosen for each experiment are listed in Tab. 1. Ratio R was calculated by assuming that HDB-LV contains 23.5 wt % of isocyanate groups and each amine molecule contains two available amino groups: $R = n_{NCO}/n_{NH_2}$, where n_{NCO} is the total amount of isocyanate groups and n_{NH_2} the total amount of amine groups.

The pH was tracked through time using a pH probe (SevenCompact, Mettler Toledo) directly plunging in the aqueous phase. Measurements were taken until the pH value stabilized.

2.4 Characterization of the Microcapsules

The size distribution of the capsules was measured precisely with a Mastersizer 3000 granulometer (Malvern), which gives the exact distribution of capsule diameters thanks to the dispersion angle of a laser beam after it encounters different particles. Lastly, the microcapsules were observed by scanning electron microscopy (SEM; EVO 15, Zeiss) to better visualize their surface aspect.

3 The Model

3.1 Description

A classical and easy way to follow the reaction rate of IP is to track the pH of the aqueous phase through time. Various models of serial mass resistances for the amine monomers have been developed [7, 11–14]. Here, a model for the specific case of $R < 1$ is developed.

A schematic of the capsule formation with a simplified view of the amine concentration profile is shown in Fig. 3. It consists of concentric radial layers of aqueous phase, aqueous film, polyurea film, and organic phase. Each interface is characterized by an equilibrium constant of concentrations: K_0 for water/polyurea (W/P) and K_i for polyurea/organic phase (P/O); C_{Ai} is the concentration of HDB-LV monomer (monomer A) in the organic phase, C_T the concentration of total amine (monomer B) in the aqueous phase, C_B the concentration of unprotonated amine in the polymer film, C_{BS} the concentration of unprotonated amine at the outer surface of the shell, and C_{Bi} the concentration at the interface between polymer and toluene. Vector $\vec{\mathbf{x}}$ has its origin at the W/P interface

Table 1. Parameters used and names of the set of experiments.

Amine	T [°C]	C_{A0} [organic phase wt %][a)]	C_{T0} [aqueous phase wt %][b)]	V_E [mL]	$R = n_{NCO}/n_{NH_2}$ [–]	Run
EDA	60	20	0.05	3	0.33	EDA 0.33
EDA	60	30	0.05	3	0.49	EDA 0.49
EDA	60	40	0.05	3	0.66	EDA 0.66
EDA	60	50	0.05	3	0.82	EDA 0.82
EDA	40	30	0.05	3	0.66	EDA 0.49 40 °C
EDA	80	30	0.05	3	0.66	EDA 0.49 80 °C
GUA	60	30	0.1	4	0.49	GUA 0.49
GUA	60	40	0.1	4	0.66	GUA 0.66
GUA	60	50	0.1	4	0.82	GUA 0.82
EDA	60	10	0.0125	3	0.66	EDA 0.66’
GUA	60	20	0.05	4	0.66	GUA 0.66’
HMDA	60	30	0.1	3	0.49	HMDA 0.49
HMDA	60	40	0.1	4	0.87	HMDA 0.87

[a)] Weight percentage of total HDB-LV in the toluene phase. Later converted to molar concentration for the rest of the paper. [b)] Weight percentage of amine in the water phase. Also converted to molar concentration further on.

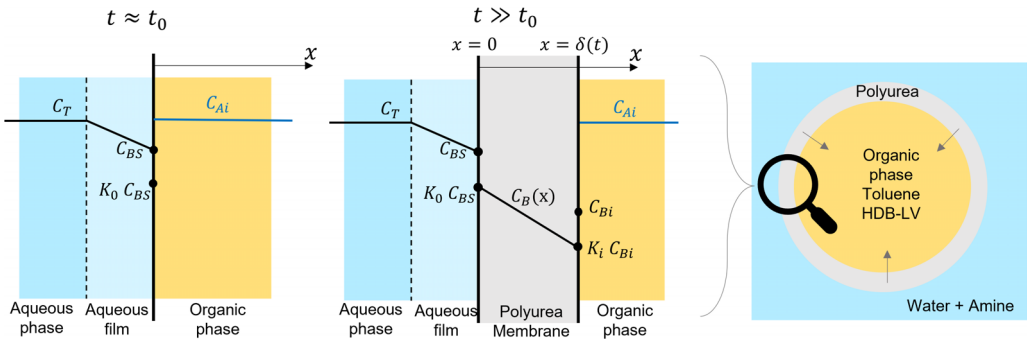

Figure 3. Schematic illustration of the amine and HDB-LV concentration through time and space in a microcapsule.

and points towards the center of the microcapsule. The increasing thickness of the entire polyurea shell is written as $\delta(t)$.

The model relies on important assumptions:

- The organic phase containing monomer A is dispersed in the form of identical drops of constant diameter d_P. Kubo et al. [11] compared the use of the mean of the dispersion and the exact distribution and showed that the results are not affected.
- Since the microcapsules are sufficiently small, the Reynolds number is so small that the Sherwood number for mass transfer in the water phase is 2.
- The shell forms towards the inside only, as monomer A has a very low affinity for water and is too big to diffuse through the polyurea shell [15, 18].
- Only the unprotonated form of the amine can diffuse through the polymer shell [7, 11, 13, 14].
- The thickness δ of the shells is negligible compared with their diameter d_P [8]. Therefore, an approximation of planar geometry is made (Fig. 3).
- Monomer B follows pseudo-steady diffusion through the polymer, so the concentration has a linear profile along the $\vec{\mathbf{x}}$ axis in the polyurea membrane due to the planar geometry.
- The kinetics between amine and isocyanate is of first order for each monomer [7, 11, 13, 14].
- The resistance to the internal transfer of HDB-LV monomer is neglected. Therefore, it is considered that there is no organic film close to the P/O interface [11, 13].

3.2 The Equations

For readability, the same notations as used by Yadav et al. are kept [13].

The hydrogen ion concentration is named $h = [H^+]$, and $H = h/h_0$ is the normalized hydrogen ion concentration, where h_0 is the initial value of h. H follows Eq. (1):

$$H = 10^{-\mathrm{pH}+\mathrm{pH}_0} \tag{1}$$

Where pH_0 is the initial value of the pH at t_0.

An important preliminary step is the linearization of pH versus total amine concentration in the water phase. Experimental curves show that the concentration of total amine C_T in Eq. (2) is a function of h involving two constants $\hat{A}$ and p that are determined for each amine later.

$$C_\mathrm{T} = \hat{A}h^{-\mathrm{p}} \tag{2}$$

Also, the concentration of unprotonated amine in the water C_{Bb} can be linked to the concentration of total amine C_T using ionic equilibrium constants (Eq. (3)):

$$C_\mathrm{Bb} = \frac{C_\mathrm{T}}{1 + \dfrac{h}{K_{a2}} + \dfrac{h^2}{K_{a1}K_{a2}}} \tag{3}$$

where K_{a2} and K_{a1} are the equilibrium constants of Eqs. (4) and (5), respectively:

$$H_3^+N - R - NH_3^+ \rightleftharpoons H_3^+N - R - NH_2 + H^+ \tag{4}$$

$$H_3^+N - R - NH_2 \rightleftharpoons NH_2 - R - NH_2 + H^+ \tag{5}$$

If $C_B(x,t)$ is the concentration of amine at a distance x from the interface between water and polymer, Eq. (6) can be written under the pseudo-steady diffusion hypothesis:

$$D_\mathrm{B}\frac{\mathrm{d}^2C_\mathrm{B}}{\mathrm{d}x^2} = 0 \tag{6}$$

where D_B is the diffusion coefficient of the unprotonated amine through the polyurea membrane.

At both interfaces, we have for $x = 0$ (Eq. (7)) and $x = \delta(t)$ (Eq. (8)):

$$C_\mathrm{B}(0,t) = K_0C_\mathrm{Bs} \tag{7}$$

$$C_\mathrm{B}(\delta(t),t) = K_\mathrm{i}C_\mathrm{Bi} \tag{8}$$

A flux balance at the reaction surface gives Eq. (9):

$$-D_\mathrm{B}\frac{\mathrm{d}C_\mathrm{B}}{\mathrm{d}x}\bigg|_\delta = k'C_\mathrm{Bi}C_\mathrm{Ai} \tag{9}$$

where k' is the surface reaction rate constant of the polymerization reaction. Because of the hypothesis of first-order reaction for each monomer, C_{Bi} and C_{Ai} appear to the power one.

The conversion of isocyanate groups to polyurea links δ and C_{Ai}, the concentration of monomer A (Eq. (10)):

$$\left(\frac{6V_d\rho}{d_p\alpha}\right)\delta = MV_d(C_{Ai} - C_{A0}) \tag{10}$$

where V_d is the volume of the dispersed organic phase, ρ the density of the polyurea, α the volume swelling factor of the polyurea, and M the molar mass of the polyurea units relative to one NCO group.

Equating the rate of change of amine concentration in the external phase to the rate of external mass transfer and in turn to the rate of uptake by the forming capsules gives Eq. (11):

$$\begin{aligned} -V_c\frac{dC_T}{dt} &= k_L\hat{a}V_c(C_{Bb} - C_{Bs}) \\ &= \left(-\frac{6V_d}{d_pVc}D_B\frac{dC_B}{dx}\bigg|_0\right)V_c \end{aligned} \tag{11}$$

where V_c is the volume of continuous aqueous phase, k_L the external mass transfer coefficient for HDB-LV, and $\hat{a}$ the interfacial area per unit volume of the continuous phase.

Eqs. (3)–(11) were combined as explained by Yadav et al. [13]. Replacing the numerous intermediate constants used in their work leads to (Eq. (11)):

$$\frac{dH}{dt} = \frac{(1/H + K_1 + K_2H)^{-1}}{\frac{p}{k_L\hat{a}} + p\left(\frac{d_pV_c}{6V_d}\right)^2\left(\frac{\alpha MC_{T0}}{\rho K_0D_B}\right)(1 - H^{-p}) + \frac{pd_pK_iV_cR}{6k'K_0C_{A0}V_d}H^p/[(R-1)H^p + 1)]} \tag{12}$$

where p is the constant calculated in Eq. (2), $K_1 = h_0 / K_{a2}$ and $K_2 = h_0^2/(K_{a1}K_{a2})$ for EDA and HMDA. For GUA, $K_1 = h_0 / K_{a1}$ and $K_2 = 0$, because this amine only dissociates once and does not follow Eq. (4).

Eq. (12) gives a numerical relationship between H and time t. It is possible to separate the variables to integrate it and get an analytical expression of t versus H.

$$\begin{aligned} t = {} & \frac{p}{k_L\hat{a}}\left[\ln H + K_1(H-1) + \frac{K_2}{2}\left(H^2-1\right)\right] + p\left(\frac{d_pV_c}{6V_d}\right)^2\left(\frac{\alpha MC_{T0}}{\rho K_0D_B}\right) \\ & \left[\ln H + K_1(H-1) + \frac{K_2}{2}\left(H^2-1\right) + \frac{H^{-p}-1}{p} + \frac{K_1}{p-1}\left(H^{-p+1}-1\right) - \right. \\ & \left. \frac{K_2}{2-p}\left(H^{2-p}-1\right)\right], \\ & + \frac{pd_pK_iV_c\,R}{6k'K_0C_{A0}V_d} \\ & \left[\frac{1}{(R-1)p}\ln\left(\frac{(R-1)H^p+1}{R}\right) + K_1\int_1^H\left(\frac{H^p}{(R-1)H^p+1}\right)dH + \right. \\ & \left. K_2\int_1^H\left(\frac{H^{p+1}}{(R-1)H^p+1}\right)dH\right] \end{aligned} \tag{13}$$

Nevertheless, due to the large values of $k_L\hat{a}$ in our experiments, we find in agreement with [13, 14] that the first term is negligible compared with the other two. Hence, Eq. (13) can be simplified to Eq. (14):

$$t = p\left(\frac{d_pV_c}{6V_d}\right)^2\left(\frac{\alpha MC_{T0}}{\rho K_0D_B}\right)f(H) + \frac{pd_pK_iV_c\,R}{6k'K_0C_{A0}V_d}g_R(H) \tag{14}$$

with

$$f(H) = \left[\begin{array}{l} \ln H + K_1(H-1) + \frac{K_2}{2}(H^2-1) + \frac{H^{-p}-1}{p} + \\ \frac{K_1}{p-1}\left(H^{-p+1}-1\right) - \frac{K_2}{2-p}\left(H^{2-p}-1\right) \end{array}\right] \tag{15}$$

and

$$g_R(H) = \left[\begin{array}{l} \frac{1}{(R-1)p}\ln\left(\frac{(R-1)H^p+1}{R}\right) + K_1\int_1^H\left(\frac{H^p}{(R-1)H^P+1}\right) \\ dH + K_2\int_1^H\left(\frac{H^{p+1}}{(R-1)H^p+1}\right)dH \end{array}\right] \tag{16}$$

Eq. (14) is the basis for the following sections of the article. The desired theoretical relation between H and time has been obtained. All the parameters found in the literature or that need to be calculated are detailed in Tab. S1 in the Supporting Information.

3.3 Using the Functions *f* and g_R to Determine the Regime of the Reaction

Eq. (14) is composed of two terms: a diffusive term with D_B and $f(H)$ and a kinetic term with k' and $g_R(H)$. If the plot of time versus $g_R(H)$ is linear during the whole experiment, then the reaction is driven by a kinetic regime. However, if after some time the plot of time versus $f(H)$ is linear until the end of the experiment, then at this point the reaction is driven by a diffusion regime. A combination of the two regimes is possible.

There is necessarily a pure kinetic regime at the start, as no polyurea has formed yet. The linearity, partial linearity, or non-linearity of the time versus $g_R(H)$ and $f(H)$ plots reveals the regime of the reaction.

4 Results and Discussion

4.1 Preliminary Estimation of *p*

To calibrate the pH probe and calculate the parameter p of Eq. (2) for different amines, the pH values for known concentrations of EDA, GUA, and HMDA at a fixed temperature were plotted. Each experimental curve was repeated twice. The plots obtained at 60 °C are shown in Fig. 4. The mass concentration of amine was converted to molar concentration [kmol L^{-1}] to calculate p, summarized in Tab. 2. The p value of 1.6 for HMDA is consistent with the literature values of 1.49 [15] and 1.71 [11].

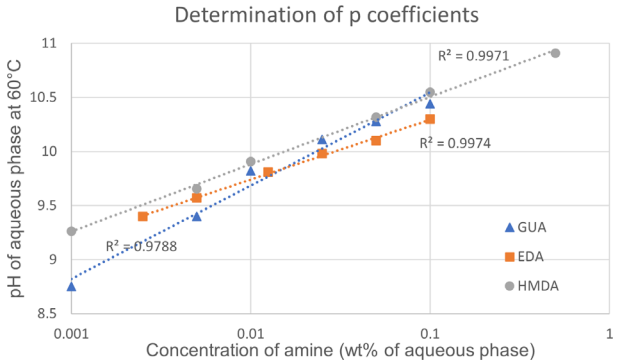

Figure 4. Estimation of the *p* parameter thanks to the calibration of the pH probe for EDA, GUA, and HMDA at 60 °C.

Table 2. Parameters relative to each amine measured in Fig. 4.

Amine	Calculated *p* coefficient [–]
GUA	1.14 ± 0.01
EDA	1.805 ± 0.005
HMDA	1.606 ± 0.005

4.2 Preliminary Estimation of d_P

The plots obtained using granulometry show a consistent size distribution among microcapsules (Fig. 5A). Other plots are not shown for the sake of visibility, as they are also superposed on the presented data. The mean diameter of microcapsules was $d_P = 0.55\,\mu m$ with a typical dispersion of 400 nm. Fig. 5B offers a visual confirmation of the value of d_P through SEM. The synthesized capsules had the same smooth aspect for all the amines used.

4.3 The pH Curves Obtained

The pH of the aqueous phase was measured every few seconds with the pH probe, and some relevant plots are presented in Fig. 6. Fig. 6A shows the effect of changes in molar ratio R with a fixed initial concentration of 0.05 wt % of EDA in the water phase. As expected, an increase of the molar ratio R results in a lower final value of the pH due to the larger amount of amine consumed by the IP. Similar results are observed for HMDA, but they are not presented in the figure for the sake of visibility. All reaction times for EDA and HMDA were around 800–1000 s.

On the other hand, Fig. 6B shows how GUA has reaction times of ca. 8000 s. The reason for this much slower reaction is not known for sure. However, a main hypothesis is that guanidine mostly exists in its protonated form as guanidinium ion in the aqueous phase, as its pK_a is 13.6. Thus, only a small minority of the amine is unprotonated and can diffuse towards the inside of the polyurea shell during IP.

4.4 The Plot of *H* and the Influence of Temperature

Using Eq. (1), it is easy to convert raw pH curves to H plots versus time; H is a normalized variable that is equal to unity at t_0 by definition. This property allows different experiments to be compared, even if their initial pH differs. For example, Fig. 7 shows the H curves obtained for EDA (R = 0.49) at different temperatures. Clearly, the final threshold value is obtained much faster at 80 °C (200 s) than at 60 °C (500 s) or 40 °C (1000 s). The fact that the value of this threshold ($H \approx 1.4$) is consistent among the different plots shows that the final concentration of amine is the same no matter the temperature of the reaction. It also shows the great repeatability of the experiments.

4.5 Defining an Experimental Molar Ratio R_{exp} using *H*

Here, the importance of the parameter R in the function $g_R(H)$ detailed in Eq. (16) is emphasized. As $R < 1$ in the experiments, small changes in R induce large numerical variations in the function $g_R(H)$ because $R - 1$ appears in fraction denominators. More importantly, R must satisfy $(R - 1)H^p + 1 > 0$ at all times to avoid divergence of the function.

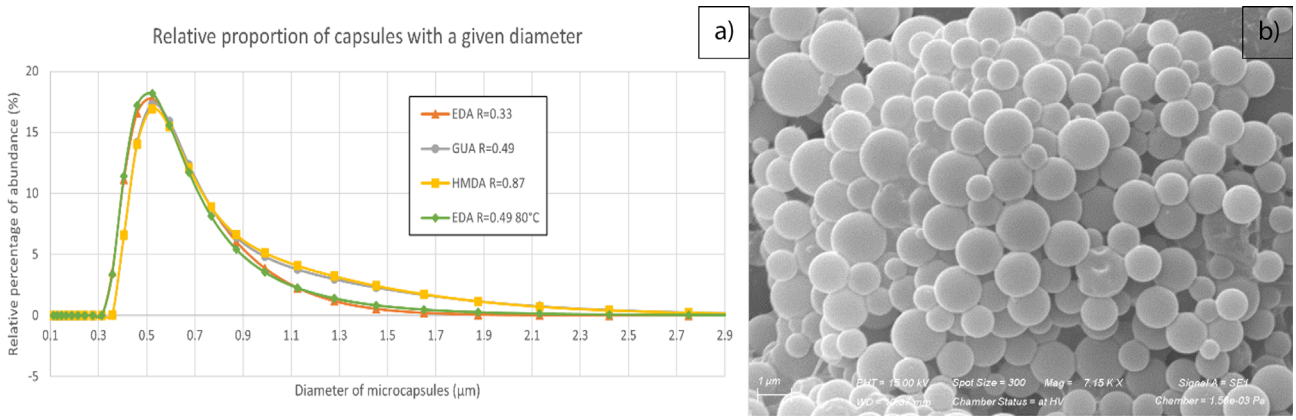

Figure 5. (a) Distribution of the diameters among the synthesized microcapsules obtained by granulometry for different amines. (b) SEM observation of dried microcapsules from the protocol for the EDA 0.49 experiment.

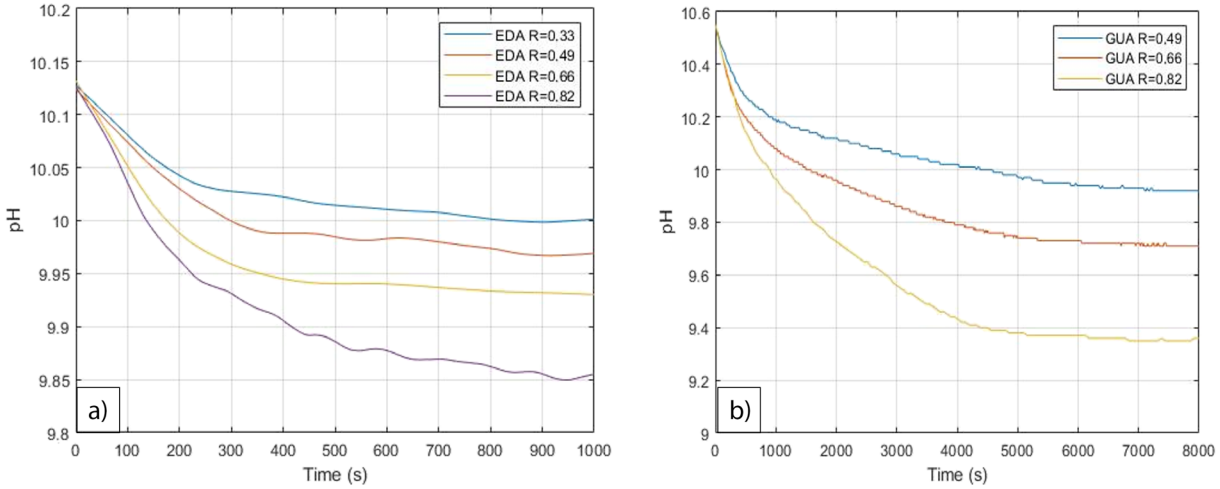

Figure 6. pH curves obtained for different experimental protocols over time. First for a fixed concentration of EDA at 0.05 wt % where *R* varies between 0.33 and 0.82 (a), and then for a fixed concentration of GUA at 0.1 wt % where *R* varies between 0.49 and 0.82 (b).

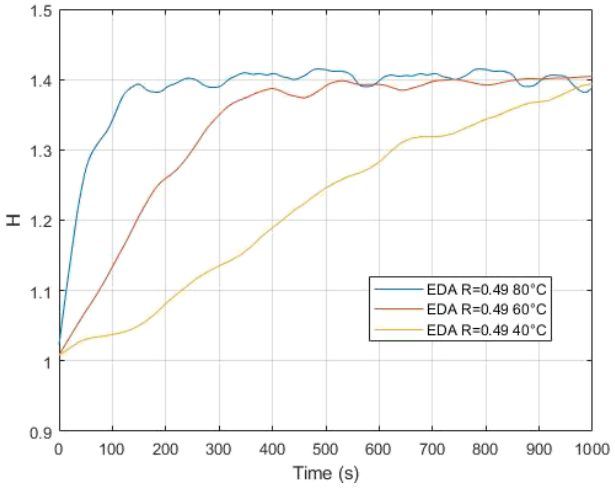

Figure 7. *H* plots derived from the raw pH curves of the experiments performed with 0.05 wt % of EDA and *R* = 0.49 at 40, 60, and 80 °C.

If during an experiment more amine is consumed than expected, the model crashes. Indeed, the amine is not supposed to keep being consumed when no more isocyanate is available for the IP. This issue is not often observed with EDA and HMDA but consistently encountered for GUA plots. The most probable explanation is that not all NH_2 groups of the GUA molecules react with NCO groups of HDB-LV, so that some GUA molecules only bond with one isocyanate monomer instead of two. However, this hypothesis is questionable, because SEM observations of GUA microcapsules did not show any difference in polyurea shape compared with other amines.

To avoid divergence, a numerical alternative solution is proposed. Using the notable result that H_f, the predicted experimental value of *H* at the end of the experiment, can be directly linked to the value of *R* under the hypothesis $V_E \ll V_2$ (Eq. (17)):

$$H_f = (1 - R)^p \tag{17}$$

Eq. (17) is used to introduce a new experimental ratio $R_{exp} = 1 - H_f^{-p}$ that can be directly calculated from the experimental value of H_f. The obtained values of R_{exp} for all experiments are listed in Tab. 3. Using R_{exp} instead of *R* in the model avoids crashing of the code when calculating $g_R(H)$. This extra step is not described by other authors, as they work with $R > 1$ and the condition $(R - 1)H^p + 1 > 0$ is always satisfied [11, 13, 14]. For industrial applications that satisfy $R < 1$, a simple calculation of R_{exp} can be used to check whether the initial molar ratio of NCO to NH_2 groups corresponds to expectation.

4.6 Estimation of *k'* and D_B Parameters Using R_{exp}

To begin the analysis of the experiments, $g_R(H)$ and $f(H)$, as defined in Eq. (14), were plotted versus time, and R_{exp} was used as the value for *R* in the expression of the function $g_R(H)$ for the reasons explained in Sect. 4.5.

The first plot of time versus $g_R(H)$ in Fig. 8A shows a linear fit during the whole experiment. According to Sect. 3.3, the IP occurs in a pure kinetic regime. Fig. 8B confirms that no significant diffusion regime exists. This is consistent over all HMDA and EDA experiments. In the case of GUA, as shown in Fig. 9A, the plot initially sticks to a linear regression but shifts away to lower slopes after 2000 s. The regime is no longer purely kinetic; it is a combination of kinetic and diffusion: the plot of time versus $f(H)$ in Fig. 9B does not show a linear plot until the end of the experiment. No pure diffusion regime was encountered in the present study.

For all the experiments, no matter the regime identified, the initial slopes of the plots in Figs. 8A and 9A were used to calculate kinetic coefficients. Indeed, Eq. (14) predicts a slope of $(pd_pK_iV_cR)/(6k'K_0C_{A0}V_d)$. This slope was estimated with Matlab, then the value of $k'K_0/K_i$ was calculated, and then *k'*. For GUA experiments, the values of *k'* and D_B were estimated with the Golden Search method. Using different values of D_B and the calculated value of *k'*, fictive plots of *H* versus time

Table 3. Experimental kinetic parameters.

Run	R_{exp} [–]	$k'K_0/K_i$ [$m^4kmol^{-1}s^{-1}$]	k' [$m^4kmol^{-1}s^{-1}$]	D_B [m^2s^{-1}]	r^2 [–]
EDA 0.33	0.37	5.83×10^{-6}	2.33×10^{-4}	$>10^{-16}$ [a]	0.995
EDA 0.49	0.51	5.28×10^{-6}	2.11×10^{-4}	$>10^{-16}$ [a]	0.975
EDA 0.66	0.60	9.65×10^{-6}	3.86×10^{-4}	$>10^{-16}$ [a]	0.988
EDA 0.82	0.78	9.28×10^{-6}	3.71×10^{-4}	$>10^{-16}$ [a]	0.997
EDA 0.49 40 °C	0.52	2.50×10^{-6}	1.00×10^{-4}	$>10^{-16}$ [a]	0.998
EDA 0.49 80 °C	0.49	1.87×10^{-5}	7.46×10^{-4}	$>10^{-16}$ [a]	0.967
GUA 0.49	0.84	2.09×10^{-3}	1.12×10^{-4}	5.0×10^{-14}	0.986
GUA 0.66	0.89	4.10×10^{-3}	2.18×10^{-4}	8.5×10^{-14}	0.971
GUA 0.82	0.95	(4.55×10^{-2}) [b]	(2.43) [b]	(9.0×10^{-14}) [b]	(0.892) [b]
EDA 0.66'	0.67	2.23×10^{-5}	8.92×10^{-4}	$>10^{-16}$ [a]	0.986
GUA 0.66'	0.85	5.01×10^{-3}	2.67×10^{-1}	1.4×10^{-14}	0.976
HMDA 0.49	0.40	1.37×10^{-5}	2.73×10^{-4}	$>10^{-16}$ [a]	0.965
HMDA 0.87	0.83	1.37×10^{-5}	2.73×10^{-4}	$>10^{-16}$ [a]	0.979

[a] Could not be determined more precisely because of the pure kinetic regime. [b] Results from the Golden Search algorithm, which gave an unreliable fit with a low value of r^2. A more coherent value of $k' = 2.4\times10^{-1}$ $m^4kmol^{-1}s^{-1}$ was retrieved from the plot of time vs $g_R(H)$ in the initial pure kinetic regime, but no suitable D_B value could be estimated to allow an accurate fit of the H curve for GUA 0.82.

were computed, and that which showed the closest similarity to the experimental data was kept. This similarity is estimated with the correlation factor r^2 defined in Eq. (18), which is maximized:

$$r^2 = 1 - \frac{\sum_i (H_i - H_{calc\,i})^2}{\sum_i (H_i - \hat{H})^2} \quad (18)$$

where H_i is the ith experimental value of H, $H_{calc\,i}$ the ith value calculated with a fixed value of k' and D_B with the model, and $\hat{H}$ the mean of all H_i values.

The optimal plots of H versus time obtained with this algorithm are shown for EDA in Fig. 8C and for GUA in Fig. 9C. Only the kinetic term is plotted in Fig. 8C because of the pure kinetic regime. It was found for EDA and HMDA that adding a diffusion term with $D_B > 10^{-16}$ m^2s^{-1}does not affect the r^2 value of the plot because of the large difference between $f(H)$ and

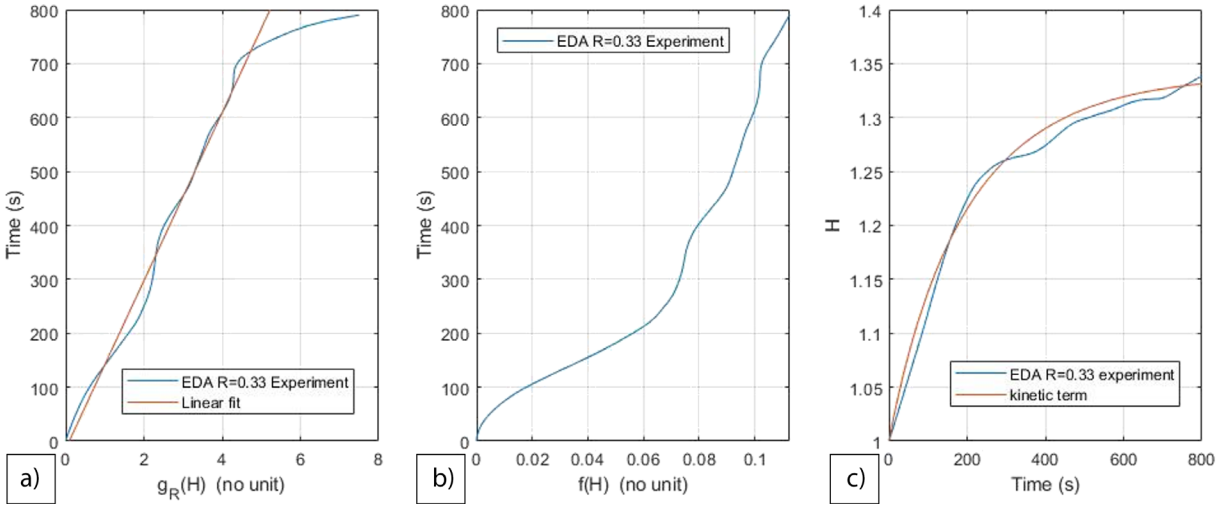

Figure 8. Kinetic plots for the experiment EDA 0.33, typically showing a full kinetic regime. First, time is plotted versus $g_R(H)$ with the linear fit that allows the constant k' to be retrieved and the duration of the kinetic regime (a). Then time is plotted versus $f(H)$ to see if there is a notable diffusion regime (b). D_B cannot be precisely calculated in this case. Finally, the retrieved fit of H versus time calculated by our theoretical model with a pure kinetic term using the calculated constant k' is shown (c).

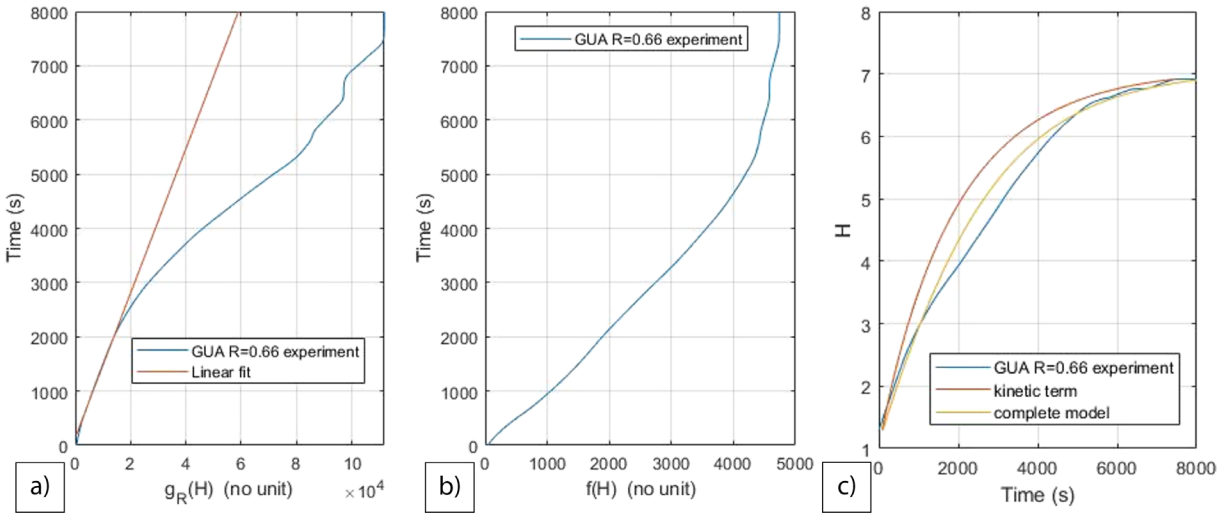

Figure 9. Kinetic plots for the experiment GUA 0.66, which follows a combination of kinetic and diffusion regimes. First, time is plotted versus $g_R(H)$ with a linear fit of the slope close to the origin, which allows the constant k' and the duration of the kinetic regime to be retrieved (a). Then, $f(H)$ is plotted versus time to see if there is a notable diffusion regime (b). There is no pure diffusion regime, but the diffusion term of Eq. (14) is not negligible in this case. Finally, the retrieved fit of H versus time calculated by our theoretical model with the estimated coefficient k' and D_B is shown. Along with the complete model, the pure kinetic component is plotted for comparison (c).

$g_R(H)$. Hence, D_B cannot be estimated more precisely. All estimated k', D_B, and r^2 for each experiment are listed in Tab. 3.

The kinetic constants k' for EDA and HMDA at 60 °C have values of about 10^{-4} m^{4}kmol^{-1}s^{-1}, using the calculated K_0 and K_i values of Tab. S1. These values of k' agree with those of Dhumal et al. [14]. However, if we use the value of $K_i = 2.06\times10^{-3}$ found by Kubo et al. [11] (but without explanation), we obtain k' values of about 10^{-7} m^4 kmol^{-1}s^{-1} like they do in the same article. Thus, our values of $k'K_0/K_i$ are always coherent regardless of the choice of K_i. We believe that they are more useful for further studies than just k' and therefore we also present them in Tab. 3.

The diffusion coefficients cannot be precisely estimated for EDA and HMDA, but values of around 10^{-14} m^{2}s^{-1} are found in the literature [13]. Surprisingly, we obtain larger kinetic constants of around 10^{-1} m^{4}kmol^{-1}s^{-1} for GUA. The diffusion coefficients reach values of around 5×10^{-14} m^{2}s^{-1}, as expected. Even if the kinetic constant is large, the pK_a value of GUA seems to be the prevalent slowing factor for the plots observed in Fig. 6B, as it limits the concentration of monomer B at P/O interface.

In the experiments EDA 0.49 40 °C, EDA 0.49 60 °C, and EDA 0.49 80 °C, the kinetic constant increases with increasing temperature, from 1.00×10^{-4} to 7.46×10^{-4} m^{4}kmol^{-1}s^{-1}. These results show that the kinetic constant of the reaction follows a classical Arrhenius law in the form of Eq. (19):

$$k' = \hat{C}e^{-\frac{E_a}{\hat{R}T}} \tag{19}$$

where $\hat{C}$ is an arbitrary constant, $\hat{R}$ the gas constant, E_a the activation energy, and T the temperature.

Following Eq. (19), a linear fit of the plot of ln(k') versus $-1/(\hat{R}T)$ gives E_a = 46 kJ mol^{-1} for the IP reaction with HDB-LV and EDA. The correlation coefficient is 0.97.

5 Conclusion

Polyurea microcapsules of reproducible size dispersion were synthesized by using EDA, HMDA, and GUA with HDB-LV monomer. Because the temperature was raised to 60 °C, it is important to fix $R < 1$ to avoid the parasitic hydrolysis of isocyanate.

In this specific case, $H_f = (1–R)^p$, so it is possible to check whether the experimental molar ratio is consistent with the estimated ratio. For the case of GUA, a constant mismatch was observed between the two values. In the future, other amines of similar molecular structure but lower pK_a will be tested under the same conditions to better understand the possible causes of the mismatch.

Considering the presented model, kinetic constants of around 10^{-4} m^{4}kmol^{-1}s^{-1} were measured for EDA and HMDA, and 10^{-1} m^{4}kmol^{-1}s^{-1} for GUA. The D_B coefficient ranged around 5×10^{-14} m^{2}s^{-1} for GUA, but its high pK_a of 13.6 might be the main cause of the extremely slow IP reaction rates observed.

So far, HDB-LV shows acceptably fast kinetics with linear diamines. The temperature changes the reaction rate, as k' follows an Arrhenius law with an activation energy of 46 kJ mol^{-1}. For all the reasons explained in this study, HDB-LV is a promising nontoxic alternative to HDI for the IP of polyurea microcapsules.

Supporting Information

Supporting Information for this article can be found under DOI: https://doi.org/10.1002/ceat.202200543. This section includes additional references to primary literature relevant for this research [19, 20].

Acknowledgment

The authors wish to thank B. Montagnier and J.-C. Hubaud for their advice in cosmetic applications of polyurea microcapsules and their synthesis. They also acknowledge G. Franco-Lage for making some of the presented IP experiments, J. Labille for his kind advice on the granulometer, A. Tonetto for the realization of the MEB pictures, and K. Ohanessian for her help with the picnometer. This work was funded by an Emplois Jeunes Doctorants grant provided by a collaboration between Region Sud (Provence Alpes Côte d'Azur) and Helioscience®.

The authors have declared no conflict of interest.

Symbols used

$\hat{a}$	[m^{-1}]	surface area per unit volume of dispersed phase
$\hat{A}$	[–]	arbitrary constant
$\hat{C}$	[–]	arbitrary constant
C_{A0}	[kmol m^{-3}]	initial concentration of HDB-LV in toluene
C_{Ai}	[kmol m^{-3}]	concentration of HDB-LV in toluene versus time
C_B	[kmol m^{-3}]	concentration of monomer B in the polymer film
C_{B0}	[kmol m^{-3}]	initial concentration of unprotonated amine
C_{Bb}	[kmol m^{-3}]	concentration of unprotonated amine in water
C_{Bi}	[kmol m^{-3}]	concentration of monomer B at P/O interface
C_{BS}	[kmol m^{-3}]	concentration of monomer B at W/P interface
C_T	[kmol m^{-3}]	concentration of total amine in the aqueous phase
C_{T0}	[kmol m^{-3}]	initial concentration of total amine in aqueous phase
D	[$m^2 s^{-1}$]	amine molecular diffusivity in water
D_B	[$m^2 s^{-1}$]	diffusion coefficient of monomer B through the polyurea shell
d_p	[m]	average microcapsule diameter
E_a	[J mol^{-1}]	activation energy
$f(H)$	[–]	numerical diffusion regime function
$g_R(H)$	[–]	numerical kinetic regime function
h	[kmol m^{-3}]	hydrogen ion concentration
H	[–]	normalized concentration of H^+ ions
$\hat{H}$	[–]	mean of all H_i values
h_0	[kmol m^{-3}]	initial hydrogen ion concentration
H_{calci}	[–]	*i*th H value calculated with a fixed value of k' and D_B with the model
H_f	[–]	final experimental value of H in a plot
H_i	[–]	*i*th experimental value of H
K_0	[–]	partition coefficient of monomer B at W/P interface
K_1	[–]	constant for each amine
K_2	[–]	constant for each amine
K_{a1}	[–]	equilibrium constant of Eq. (5)
K_{A2}	[–]	equilibrium constant of Eq. (4)
K_i	[–]	partition coefficient of monomer B at P/O interface
k_L	[m s^{-1}]	external mass transfer coefficient for monomer B
k'	[$m^4 kmol^{-1} s^{-1}$]	surface reaction rate constant of the polymerization reaction
M	[kg $kmol^{-1}$]	polyurea molar mass
M_A	[kg $kmol^{-1}$]	HDB-LV molar mass (normalized to one NCO group)
M_B	[kg $kmol^{-1}$]	amine molar mass
n_{NCO}	[kmol]	number of total isocyanate groups
n_{NH_2}	[kmol]	number of total amine groups
p	[–]	constant for each amine
R	[–]	molar ratio of NCO/NH_2 groups
r^2	[–]	correlation factor
$\hat{R}$	[J $mol^{-1} K^{-1}$]	gas constant
R_{exp}	[–]	retrieved experimental molar ratio
t	[s]	time
T	[K]	temperature
t_0	[s]	initial time
t_f	[s]	final time
V_1	[m^3]	emulsion volume
V_2	[m^3]	volume of aqueous amine solution
V_c	[m^3]	volume of continuous phase
V_d	[m^3]	volume of dispersed phase
V_E	[m^3]	volume of emulsion poured into the water + amine phase
x	[m]	distance to the W/P interface
$\vec{\mathbf{x}}$	[m]	vector with origin at W/P interface pointing towards the center of the microcapsule

Greek letters

α	[–]	volume swelling factor of polyurea
δ	[m]	thickness of polyurea shell
ρ	[kg m^{-3}]	density of polyurea

Abbreviations

EDA	ethylenediamine
GUA	guanidine
HDB-LV	hexamethylene diisocyanate biuret low viscosity
HDI	hexamethylene diisocyanate
HMDA	hexamethylenediamine
IP	interfacial polymerization
Monomer A	isocyanate monomer
Monomer B	amine monomer
P/O	polyurea/organic
SDS	sodium dodecyl sulfate
SEM	scanning electron microscopy
W/P	water/polyurea

References

[1] M. J. T. Raaijmakers, N. E. Benes, *Prog. Polym. Sci.* **2016**, *63*, 86–142. DOI: https://doi.org/10.1016/j.progpolymsci.2016.06.004

[2] Y. Song, J.-B. Fan, S. Wang, *Mater. Chem. Front.* **2017**, *1 (6)*, 1028–1040. DOI: https://doi.org/10.1039/C6QM00325G

[3] I. T. Carvalho, B. N. Estevinho, L. Santos, *Int. J. Cosmet. Sci.* **2016**, *38 (2)*, 109–119. DOI: https://doi.org/10.1111/ics.12232

[4] L. Ren, B. Huang, W. Fang, D. Zhang, H. Cheng, Z. Song, D. Yan, Y. Li, Q. Wang, Z. Zhou, A. Cao, *ACS Appl. Mater. Interfaces* **2021**, *13 (1)*, 1333–1344. DOI: https://doi.org/10.1021/acsami.0c16613

[5] P. Scarfato, E. Avallone, P. Iannelli, V. De Feo, D. Acierno, *J. Appl. Polym. Sci.* **2007**, *105 (6)*, 3568–3577. DOI: https://doi.org/10.1002/app.26420

[6] R. J. Petersen, *J. Membr. Sci.* **1993**, *83 (1)*, 81–150. DOI: https://doi.org/10.1016/0376-7388(93)80014-O

[7] S. K. Karode, S. S. Kulkarni, A. K. Suresh, R. A. Mashelkar, *Chem. Eng. Sci.* **1997**, *52 (19)*, 3243–3255. DOI: https://doi.org/10.1016/S0009-2509(97)00138-3

[8] J. Du, N. Ibaseta, P. Guichardon, *Chem. Eng. Res. Des.* **2022**, *182*, 256–272. DOI: https://doi.org/10.1016/j.cherd.2022.03.026

[9] J. Du, N. Ibaseta, P. Guichardon, *Chem. Eng. Res. Des.* **2020**, *159*, 615–627. DOI: https://doi.org/10.1016/j.cherd.2020.04.012

[10] I. Polenz, D. A. Weitz, J.-C. Baret, *Langmuir* **2015**, *31 (3)*, 1127–1134. DOI: https://doi.org/10.1021/la5040189

[11] M. Kubo, Y. Harada, T. Kawakatsu, T. Yonemoto, *J. Chem. Eng. Jpn.* **2001**, *34 (12)*, 1506–1515. DOI: https://doi.org/10.1252/jcej.34.1506

[12] S. K. Yadav, A. K. Suresh, K. C. Khilar, *AIChE J.* **1990**, *36 (3)*, 431–438. DOI: https://doi.org/10.1002/aic.690360312

[13] S. K. Yadav, K. C. Khilar, A. K. Suresh, *AIChE J.* **1996**, *42 (9)*, 2616–2626. DOI: https://doi.org/10.1002/aic.690420922

[14] S. Dhumal, S. Wagh, A. Suresh, *J. Membr. Sci.* **2008**, *325 (2)*, 758–771. DOI: https://doi.org/10.1016/j.memsci.2008.09.002

[15] S. J. Wagh, S. S. Dhumal, A. K. Suresh, *J. Membr. Sci.* **2009**, *328 (1–2)*, 246–256. DOI: https://doi.org/10.1016/j.memsci.2008.12.018

[16] J. Pauluhn, *Toxicol. Sci.* **2000**, *58 (1)*, 173–181. DOI: https://doi.org/10.1093/toxsci/58.1.173

[17] Z. Chen, W. Yang, H. Yin, S. Yuan, *Chin. J. Chem. Eng.* **2017**, *25 (10)*, 1435–1441. DOI: https://doi.org/10.1016/j.cjche.2017.03.012

[18] Y. Yang, Z. Wei, C. Wang, Z. Tong, *ACS Appl. Mater. Interfaces* **2013**, *5 (7)*, 2495–2502. DOI: https://doi.org/10.1021/am302963d

[19] J. A. Dean, *Lange's Handbook of Chemistry*, 15th ed., McGraw-Hill, New York **1999**.

[20] E. D. Raczynska, M. K. Cyranski, M. Gutowski, J. Rak, J.-F. Gal, P.-C. Maria, M. Darowska, K. Duczmal, *J. Phys. Org. Chem.* **2003**, *16 (2)*, 91–106. DOI: https://doi.org/10.1002/poc.578